Co-design of a wave energy converter through bi-conjugate impedance matching

Ryan G. Coe[a,*], Giorgio Bacelli[a], Daniel Gaebele[a], Alicia Keow[a], Dominic Forbush[a]

[a]*Sandia National Laboratories, PO BOX 5800, Albuquerque, 87123, NM, USA*

Abstract

As with other oscillatory power conversion systems, the design of wave energy converters can be understood as an impedance matching problem. By representing the wave energy converter as a multi-port network, two separate but related impedance matching conditions can be established. Satisfying these conditions maximizes power transfer to the load. In practice, these impedance matching conditions may be used to influence the design of the system (including the hull, power take-off, controller, mooring, etc.). To this end, this paper considers some example applications of wave energy converter design with the help of the impedance matching framework.

Keywords: wave energy converter (WEC), control co-design, impedance matching

1. Introduction

Wave energy converters (WECs) must be designed to capture a purely oscillatory power input—this is a unique characteristic amongst most other energy generation technologies (e.g., wind turbines, hydroelectric dams, nuclear power plants). However, there are useful tools at the disposal of a WEC designer for maximizing the useful power delivered to a load in an oscillatory system from fields such as power transmission and radio-frequency engineering. The concept of impedance matching to maximize power output has been applied in wave energy since at least the 1970s [1]. For reasons that are unclear, this concept has mostly been applied only to the power conversion stage between the waves/WEC hull and the input of the power take-off (PTO) system. As will be discussed in further detail in this paper, disregarding the subsequent power conversion stages between mechanical power on the hull and useful (e.g., electrical) power at the output of the machine has a number of adverse consequences.

This concept of transferring power between the different stages of a WEC is illustrated in Figure 1. The ultimate goal of a WEC is to deliver power to a load (e.g., DC power a battery bank or pressurized water to a reverse osmosis filter for desalination). Because the source power is purely oscillatory, the power flow between the stages in Figure 1 is generally shown to be bi-directional. In fact, the optimal condition requires that half the power be reflected [2]. The conditions that ensure this optimal power transmission are shown at the top of Figure 1. The first impedance matching condition in Figure 1 ($Z_i^* = Z_{\text{in}}$) is generally well-known and widely applied in WEC engineering, although it uses somewhat different notation since

*Corresponding author
Email addresses: `rcoe@sandia.gov` (Ryan G. Coe), `gbacell@sandia.gov` (Giorgio Bacelli), `dtgaebe@sandia.gov` (Daniel Gaebele), `akeow@sandia.gov` (Alicia Keow), `dforbus@sandia.gov` (Dominic Forbush)
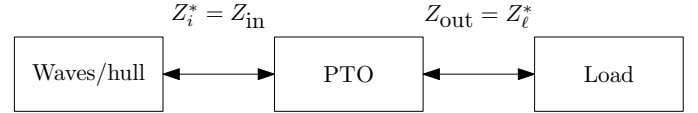
Figure 1: WEC power flow stages with impedance matching conditions.

the input/output distinction within the PTO is not widely utilized. The second impedance matching condition in Figure 1 ($Z_{\text{out}} = Z_\ell^*$) is mostly ignored and/or lumped with the first condition under the often unstated assumption that the PTO dynamics can be decoupled from the hydrodynamic system, thus limiting performance. The details of these impedance matching expressions will be addressed later in this paper.

Power delivered to the load is affected by both losses and reflections in the WEC system. These two effects are distinct and must be addressed as such. Losses are due to friction or electrical resistance – this effect is often two more intuitive of the two. Reflections, which are due to a mismatch in the system impedances, are generally underappreciated in WEC design.

This paper further explores concepts of bi-conjugate impedance matching in wave energy previously raised by [3], with the goal of generating a more practical understanding of the utility and application of this theory. First, a basic review of network modeling and elements is presented (Section 2). Next, this framework is applied to a WEC (Section 3). Finally, in a number of illustrative case studies are considered (Section 4).

2. Multi-port networks

The multi-port network models popular in electronics and microwave systems [4, 5] provide a useful construct for analyzing a WEC. Because they are utilized in many different applications, there are multiple conventions for multi-port network models – Appendix Appendix A provides further discussion on this and explains the conventions employed in this paper.

Given that these models are not currently used broadly within the wave energy field, we will now review the fundamental concepts of multi-port network models. Figure 2 provides a central reference for this discussion, with columns pertaining to different network model elements and representations/explanations of those elements shown in each row. First, let us consider one-port elements, which, as shown on the left hand side of Figure 2, relate a single effort variable (e) to a single flow variable (q) through an impedance (Z).

$$Z = \frac{e}{q} \tag{1}$$

Similarly, two-port elements relate two pairs of effort and flow variables (see the right hand side of Figure 2).[1]

$$\begin{bmatrix} e_1 \\ e_2 \end{bmatrix} = \begin{bmatrix} Z_{11} & Z_{12} \\ Z_{21} & Z_{22} \end{bmatrix} \begin{bmatrix} q_1 \\ q_2 \end{bmatrix}, \tag{2}$$

The elements of any two-port impedance matrix may be defined as follows [5].

$$Z_{11} = \frac{e_1}{q_1}\bigg|_{q_2=0} \qquad Z_{12} = \frac{e_1}{q_2}\bigg|_{q_1=0}$$

$$Z_{21} = \frac{e_2}{q_1}\bigg|_{q_2=0} \qquad Z_{22} = \frac{e_2}{q_2}\bigg|_{q_1=0} \tag{3}$$

The product of the effort and flow variables on each port is power. Note also the sign conventions illustrated in Figure 2, which result in power flow into the two-port network from both sides, summing to zero for a lossless system. In addition to the "impedance form" shown in (2), there are many equivalent formulations for modeling two-port networks [5]. Certain formulations may be easier to work with depending on the task at hand. In this paper, we will also utilize the "$ABCD$ form" (also referred to as "chain," "cascade," or "transmission" form):

$$\begin{bmatrix} e_1 \\ q_1 \end{bmatrix} = \begin{bmatrix} A & B \\ C & D \end{bmatrix} \begin{bmatrix} e_2 \\ -q_2 \end{bmatrix}, \tag{4}$$

Similarly to (3), the elements of the $ABCD$ matrix are defined as follows.

$$A = \frac{e_1}{e_2}\bigg|_{q_2=0} \qquad B = -\frac{e_1}{q_2}\bigg|_{e_2=0} \tag{5a}$$

$$C = \frac{q_1}{e_2}\bigg|_{q_2=0} \qquad D = -\frac{q_1}{q_2}\bigg|_{e_2=0} \tag{5b}$$

Note that the impedance form and $ABCD$ form matrix elements are explicitly interrelated (see, e.g., [5]). For example, we may relate the impedance and $ABCD$ forms.

$$\begin{bmatrix} Z_{11} & Z_{12} \\ Z_{21} & Z_{22} \end{bmatrix} = \frac{1}{C} \begin{bmatrix} A & \Delta[\mathbf{a}] \\ 1 & D \end{bmatrix} \tag{6}$$

Here, $\Delta[\mathbf{a}]$ is the determinant of the $ABCD$ matrix. From (6), we can see that some representations may be undefined for certain two-port elements (e.g., if $C = 0$ in the $ABCD$ form, the impedance form will be undefined).

The scattering parameters for a multi-port are also of interest to us, as they directly quantify the fraction of reflected/transmitted power.

$$\begin{bmatrix} b_1 \\ b_2 \end{bmatrix} = \begin{bmatrix} S_{11} & S_{12} \\ S_{21} & S_{22} \end{bmatrix} \begin{bmatrix} a_1 \\ a_2 \end{bmatrix} \tag{7}$$

Here, a_k and b_k are, respectively, the incoming and outgoing square root of power on the kth-port [6].[2] The scattering parameters depend on both the multi-port element and the connections at each port (e.g., the source and load impedances for a two-port) and thus are helpful in understanding the impedance matching of the mutli-port to adjacent elements.

A two-port element can be collapsed into a one-port element if one of the ports is terminated with a load and has no independent sources. Whereas the general two-port element has four variables, two of which are independent, in the scenario where one port is terminated with a load, the system loses a degree of freedom. Thus, in this case, we may simplify the system as a one-port element (i.e., a single impedance). With these general properties in hand, let us now consider some fundamental multi-port elements shown in Figure 2.

2.1. Impedances (one-ports)

To incorporate dynamics and losses into the system description, we utilize one-port impedance elements, which describe how components *impede* flow via opposing effort. In general, for a series impedance in a closed loop (see "series impedance" in Figure 2), we may write,

$$e_1 = Zq_1 + e_2 \tag{8a}$$
$$q_1 = -q_2, \tag{8b}$$

which can be equivalently represented in $ABCD$ form as,

$$\begin{bmatrix} e_1 \\ q_1 \end{bmatrix} = \begin{bmatrix} 1 & Z \\ 0 & 1 \end{bmatrix} \begin{bmatrix} e_2 \\ -q_2 \end{bmatrix}. \tag{9}$$

Alternatively, if the impedance is connected in parallel (see "shunt impedance" in Figure 2), we may write

$$e_1 = e_2 \tag{10a}$$
$$q_1 = \frac{1}{Z}e_2 - q_2, \tag{10b}$$

which can be equivalently represented in $ABCD$ form.

$$\begin{bmatrix} e_1 \\ q_1 \end{bmatrix} = \begin{bmatrix} 1 & 0 \\ \frac{1}{Z} & 1 \end{bmatrix} \begin{bmatrix} e_2 \\ -q_2 \end{bmatrix} \tag{11}$$

---

[1]As the "multi-port" name suggests, elements with more than two ports (three, four, etc.) may also be considered.

[2]The "Kurokawa power wave" scattering parameters are used here; see Appendix Appendix A for further explanation.

	One-port element		Two-port element	

	Series impedance	Shunt impedance	Transformer	Gyrator
Network diagram symbols	Z	Z	$N_p : N_s$	γ_g
Variable relationships	$e_1 = Zq + e_2$ $q = q$	$e = e$ $q_1 = \frac{1}{Z}e - q_2$	$e_1 = \gamma_t e_2$ $q_1 = \frac{-1}{\gamma_t}q_2$	$e_2 = \gamma_g q_1$ $e_1 = -\gamma_g q_2$
Examples	$I \quad R$ $\forall_1 = RI + \forall_2$	$\dot{m}_o,\ p_a$ p κ, V_a $\dot{m}_i$ $K_a = \frac{\kappa p_a}{i\omega V_a}$ $\dot{m}_i = \frac{1}{K_a}p + \dot{m}_o$	v_1, τ_1 v_2, τ_2 $N = \frac{r_1}{r_2}$ $\tau_1 = N\tau_2$ $v_1 = -\frac{1}{N}v_2$	I N_t r v_s, τ $k_\tau = 2N_t B_f \ell r$ $\tau = -k_\tau I$ $\forall = k_\tau v_s$
ABCD form $(q_{out} = -q_2)$ $q_1 \to [\mathbf{a}] \to q_{out}$	$\begin{bmatrix} e_1 \\ q_1 \end{bmatrix} = \begin{bmatrix} 1 & Z \\ 0 & 1 \end{bmatrix}\begin{bmatrix} e_2 \\ q_{out} \end{bmatrix}$	$\begin{bmatrix} e_1 \\ q_1 \end{bmatrix} = \begin{bmatrix} 1 & 0 \\ 1/Z & 1 \end{bmatrix}\begin{bmatrix} e_2 \\ q_{out} \end{bmatrix}$	$\begin{bmatrix} e_1 \\ q_1 \end{bmatrix} = \begin{bmatrix} \gamma_t & 0 \\ 0 & 1/\gamma_t \end{bmatrix}\begin{bmatrix} e_2 \\ q_{out} \end{bmatrix}$	$\begin{bmatrix} e_1 \\ q_1 \end{bmatrix} = \begin{bmatrix} 0 & \gamma_g \\ 1/\gamma_t & 0 \end{bmatrix}\begin{bmatrix} e_2 \\ q_{out} \end{bmatrix}$
Impedance form $q_1 \to [\mathbf{z}] \leftarrow q_2$	not defined	$\begin{bmatrix} e_1 \\ e_2 \end{bmatrix} = \begin{bmatrix} Z & Z \\ Z & Z \end{bmatrix}\begin{bmatrix} q_1 \\ q_2 \end{bmatrix}$	not defined	$\begin{bmatrix} e_1 \\ e_2 \end{bmatrix} = \begin{bmatrix} 0 & -\gamma_t \\ \gamma_t & 0 \end{bmatrix}\begin{bmatrix} q_1 \\ q_2 \end{bmatrix}$

Figure 2: General one- and two-port elements definition showing effort (e) and flow (q) at each port with diagrams and mathematical relationships for impedances, transformers, and gyrators.

2.2. Transformers

Electric transformers are widely known and understood to convert between different voltage levels. For an ideal transformer, we may define a constant γ_t that relates the effort and flow variables (see Figure 2).

$$e_1 = \gamma_t e_2 \tag{12a}$$

$$q_1 = -\frac{1}{\gamma_t}q_2 \tag{12b}$$

Note that, as shown in Figure 2, (12) relates the flow at port 1 to the flow at port 2 and effort at port 1 to the effort at port 2 (i.e., the flows are directly related to each other, as are the efforts). In an electric transformer, the constant γ_t is the ratio of windings on its primary and secondary sides ($\gamma_t = N_p/N_s$). A geared transmission is a mechanical example of a transformer (see Figure 2); in this case, γ_t is the gear ratio. In *ABCD* form, we may represent a transformer as

$$\begin{bmatrix} e_1 \\ q_1 \end{bmatrix} = \begin{bmatrix} \gamma_t & 0 \\ 0 & 1/\gamma_t \end{bmatrix}\begin{bmatrix} e_2 \\ -q_2 \end{bmatrix}. \tag{13}$$

Recalling (6), we may see that the impedance form representation for a transformer is not defined ($1/C \to \infty$).

2.3. Gyrators

Gyrators are effectively the opposites of transformers in that they relate the flow at one port to the effort at the other port (see Figure 2). In general, we may write

$$e_1 = -\gamma_g q_2 \tag{14a}$$

$$q_1 = \frac{1}{\gamma_g}e_2, \tag{14b}$$

where γ_g is the gyration modulus. In *ABCD* form, a gyrator can be represented as

$$\begin{bmatrix} e_1 \\ q_1 \end{bmatrix} = \begin{bmatrix} 0 & \gamma_g \\ 1/\gamma_g & 0 \end{bmatrix}\begin{bmatrix} e_2 \\ -q_2 \end{bmatrix}. \tag{15}$$

An electric motor/generator is a very relevant example of a gyrator. In that case, the gyration modulus is the motor constant
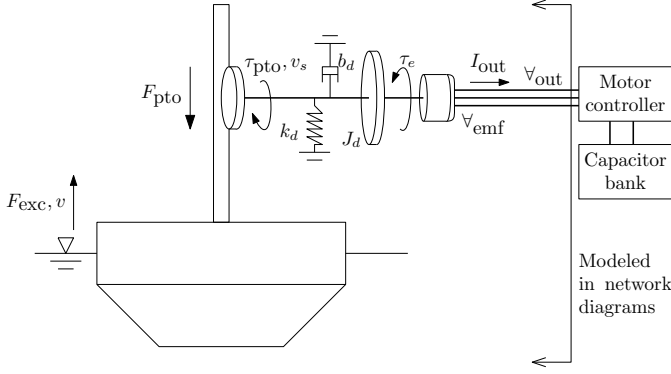
Figure 3: WaveBot device diagram.

Table 1: Key physical parameters of the WaveBot.

Parameter	Value
Rigid body mass, m [kg]	875
Hydrostatic stiffness, k_h [kN/m]	2.44
Linear friction coefficient, b_f [Ns/m]	1
Linear to rotational gear ratio, N [rad/m]	12.4666
Shaft inertia, J_d [kg m^2]	2
Shaft friction, b_d [Nm s/rad]	1
Grounded shaft spring stiffness, k_d [Nm/rad]	0
Torque constant, k_τ [Nm/A]	6.1745
Motor winding resistance, R_w [Ω]	0.5
Motor winding inductance, L_w [H]	0

($\gamma_g = k_\tau$). The direction of the arrow in a gyrator schematic as shown in Figure 2 indicates the directionality of the element: the *positive* product of the flow at the arrow's tail with the gyration modulus gives the effort at the arrow's head ($e_2 = \gamma_g q_1$ as drawn in Figure 2 with the arrow pointing from port 1 to port 2) and the effort at the arrow's tail is the *negative* product of the gyration modulus and effort at the head ($e_1 = -\gamma_g q_2$ as drawn in Figure 2). Note that a cascade of two gyrators has the composite effect of a transformer. For example, two lossless electric motor/generators with coupled shafts would be equivalent to an electrical transformer with a winding ratio of $\gamma_t = N_p/N_s = \gamma_{g1}/\gamma_{g2}$.

3. Modeling a direct drive WEC

Using the general definitions for multi-port modeling presented in Section 2, we now wish to model a WEC. To this end, let us consider the heaving buoy style "WaveBot" device with a direct drive PTO as shown in Figure 3 [7]. Table 1 lists key parameters for the WaveBot. We will first present the WEC and its governing equations in further detail (Section 3.1) and then utilize those governing equations to represent the system via multi-port network models (Section 3.2).
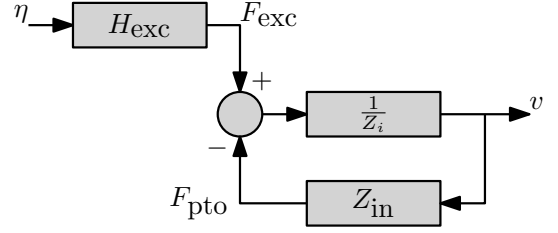

Figure 4: Generic block diagram for a wave energy converter.

3.1. Dynamic and kinematic equations

Vertical motion of the buoy can be expressed as a dynamic equation dependent on the PTO force[3] (F_{pto}), the excitation force (F_{exc}), and the intrinsic impedance (Z_i) [8].

$$F_{\mathrm{exc}} - F_{\mathrm{pto}} = Z_i v \tag{16a}$$

$$Z_i(\omega) = B(\omega) + b_f + j\left(\omega\,(m + A(\omega)) - \frac{k_h}{\omega}\right) \tag{16b}$$

Here, $A(\omega)$ is the added mass, $B(\omega)$ is the radiation damping, k_h is the hydrostatic stiffness, b_f accounts for linear friction effects, and m is the rigid body inertia. The imaginary unit is j and ω is the angular frequency. A block diagram[4] in Figure 4 shows the system described by (16a). In Figure 4, the PTO force is determined based on the PTO input impedance (Z_{in}) – the details of this will be discussed in more detail in Section 3.2.3; the excitation force (F_{exc}) is determined from the excitation transfer function (H_{exc}) based on the wave elevation (η).

The rectilinear vertical velocity (v) and force (F_{pto}) in (16a) are transformed into rotational velocity (v_s) and torque (τ_{pto}) on a rotating shaft by a "rack and pinion" style mechanism with radius N.

$$v_s = Nv \tag{17a}$$

$$\tau_{\mathrm{pto}} = \frac{1}{N} F_{\mathrm{pto}} \tag{17b}$$

Comparing (17) and (12), we may note that the rack and pinion is an example of a transformer.

The rotating drive-train shaft has characteristic linear friction (b_d), inertia (J_d), and may include some non-zero spring stiffness effect against the ground (k_d). The opposite end of the drive-train shaft interfaces with an electric motor/generator that produces an electromagnetic torque (τ_e). Thus, we may describe the drive-train dynamics as follows.

$$\tau_{\mathrm{pto}} - \tau_e = Z_d v_s \tag{18a}$$

$$Z_d = b_d + j\left(\omega J_d - \frac{k_d}{\omega}\right) \tag{18b}$$

---

[3]Note that we define the "PTO" force in the opposite direction of the excitation force and velocity as shown in Figure 3. This sign convention, where, as in (16a), we have an expression of the form $Zq = e_1 - e_2$, is most common in network diagrams and control engineering and therefore used herein.

[4]Note that block diagrams are related to but distinct from the network diagrams used elsewhere in this paper. To emphasize this distinction, a grey fill is used for blocks in Figure 4.

The electric motor/generator can be considered to have the composite characteristics of a pure gyrator and an impedance. For the gyrator element, the machine has a characteristic torque constant (gyration modulus) k_τ that relates back EMF voltage ($\forall_{\mathrm{emf}}$) to shaft speed and electromagnetic torque to the quadrature current (I_{out}) when using a Park power invariant transformation.

$$v_s = \frac{1}{k_\tau}\forall_{\mathrm{emf}} \tag{19a}$$

$$\tau_e = k_\tau I_{\mathrm{out}} \tag{19b}$$

In addition to its gyration effect, the motor has a characteristic impedance (Z_w) that captures the effects of winding resistance (R_w) and inductance (L_w), and relates the output current to the back EMF voltage ($\forall_{\mathrm{emf}}$) and output voltage ($\forall_{\mathrm{out}}$).

$$\forall_{\mathrm{emf}} - \forall_{\mathrm{out}} = Z_w I_{\mathrm{out}} \tag{20a}$$

$$Z_w = R_w + j\omega L_w \tag{20b}$$

Finally, we may define a load impedance (Z_ℓ) that represents how current is modulated by the motor controller relative to voltage.

$$Z_\ell = \frac{\forall_{\mathrm{out}}}{I_{\mathrm{out}}} \tag{21}$$

In practice, the load impedance will be defined by a controller (C). It is generally convenient to implement a feedback controller that commands motor current based on the angular velocity (I_{out} and v_s, respectively, in Figure 3).

$$I_{\mathrm{out}} = C v_s \tag{22a}$$

$$Z_\ell = \frac{1}{C}k_\tau - Z_w \tag{22b}$$

While many forms may be used for C, a simple proportional-integral (PI) structure can be quite effective [9].

$$C_{PI} = k_p + \frac{1}{j\omega}k_i \tag{23}$$

The current command in (23) is thus defined as the sum of products *proportional* to velocity ($v_s k_p$) and the *integral* of velocity ($\frac{v_s}{j\omega}k_i$, i.e., position).

3.2. Modeling with a network diagram

The WaveBot device shown in Figure 3 and described in Section 3.1 can be represented with network diagrams as shown in Figure 5. Various levels of abstraction/detail can be achieved in this style of diagram. Figure 5a shows the highest level of detail, whereas Figure 5b and Figure 5c increasingly combine elements to achieve a single two-port network to represent the PTO. We will return to Figure 5d-f for later discussion.

We now consider two equivalent approaches for producing multi-port models to represent our WEC: work from an impedance form (Section 3.2.1) and working from *ABCD* form (Section 3.2.2). These multi-port models for the WEC are then used to formulate a number of expressions useful in the WEC design problem.
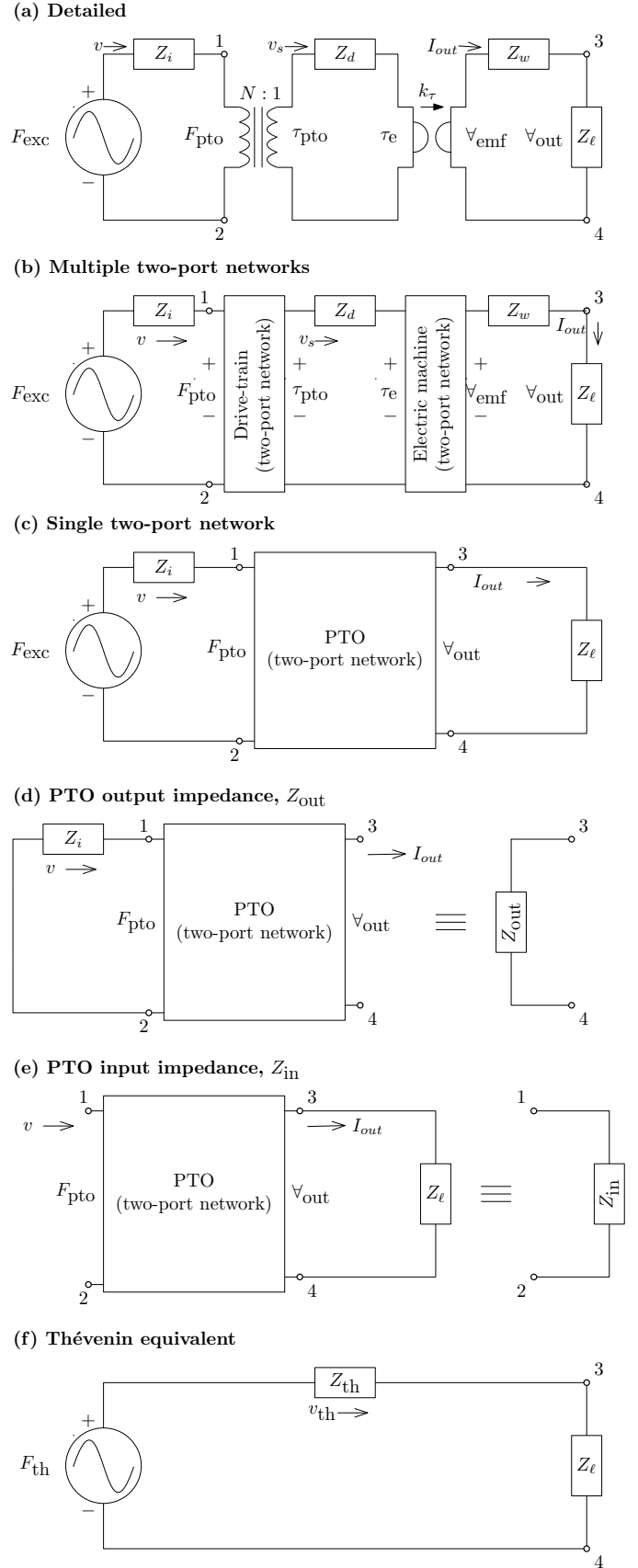

Figure 5: Circuit diagrams representing a wave energy converter. Points 1, 2, 3, and 4 are consistent throughout the different diagrams.

3.2.1. PTO impedance matrix

For the network shown in Figure 5c, we may write an impedance matrix to describe the two-port element representing the PTO.

$$\begin{bmatrix} F_{\text{pto}} \\ \forall_{\text{out}} \end{bmatrix} = \begin{bmatrix} Z_{11} & Z_{12} \\ Z_{21} & Z_{22} \end{bmatrix} \begin{bmatrix} v \\ I_{\text{in}} \end{bmatrix} \tag{24}$$

Utilizing (3) and the equations for our system of interest presented in Section 3.1, the elements of the impedance matrix in (24) may be written out as follows.

$$Z_{11} = \frac{e_1}{q_1}\Big|_{q_2=0} = \frac{F_{\text{pto}}}{v}\Big|_{I_{\text{out}}=0} = Z_d N^2 \tag{25a}$$

$$Z_{12} = \frac{e_1}{q_2}\Big|_{q_1=0} = \frac{F_{\text{pto}}}{I_{\text{out}}}\Big|_{v=0} = -k_\tau N \tag{25b}$$

$$Z_{21} = \frac{e_2}{q_1}\Big|_{q_2=0} = \frac{\forall_{\text{out}}}{v}\Big|_{I_{\text{out}}=0} = k_\tau N \tag{25c}$$

$$Z_{22} = \frac{e_2}{q_2}\Big|_{q_1=0} = \frac{\forall_{\text{out}}}{I_{\text{out}}}\Big|_{v=0} = Z_w \tag{25d}$$

Taken together, this gives

$$[\mathbf{z}]_{\text{pto}} = \begin{bmatrix} Z_{11} & Z_{12} \\ Z_{21} & Z_{22} \end{bmatrix} = \begin{bmatrix} Z_d N^2 & -k_\tau N \\ k_\tau N & Z_w \end{bmatrix}. \tag{26}$$

3.2.2. PTO transmission matrix

Alternatively, we may also represent the PTO by cascading the one- and two-port elements, as shown in the more detailed diagrams in Figure 5a and Figure 5b, to obtain an *ABCD* matrix.

$$\begin{bmatrix} F_{\text{pto}} \\ v \end{bmatrix} = \begin{bmatrix} A_{\text{pto}} & B_{\text{pto}} \\ C_{\text{pto}} & D_{\text{pto}} \end{bmatrix} \begin{bmatrix} \forall_{\text{out}} \\ I_{\text{out}} \end{bmatrix} \tag{27}$$

This is convenient because the cascading matrices are multiplied in the same order that a network diagram would be drawn, from wave-to-wire. Working from left to right in Figure 5b and using the *ABCD* matrices for transformers, gyrators, and impedances in (13), (15), and (9), respectively, we may write

$$\begin{bmatrix} F_{\text{pto}} \\ v \end{bmatrix} = \overbrace{\underbrace{\begin{bmatrix} N & 0 \\ 0 & 1/N \end{bmatrix}}_{\substack{\text{linear to} \\ \text{rotary gear} \\ \text{transformer}}} \underbrace{\begin{bmatrix} 1 & Z_d \\ 0 & 1 \end{bmatrix}}_{\substack{\text{drive-train} \\ \text{impedance}}} \underbrace{\begin{bmatrix} 0 & k_\tau \\ 1/k_\tau & 0 \end{bmatrix}}_{\substack{\text{electric} \\ \text{machine} \\ \text{gyrator}}} \underbrace{\begin{bmatrix} 1 & Z_w \\ 0 & 1 \end{bmatrix}}_{\substack{\text{winding} \\ \text{impedance}}}}^{[\mathbf{a}]_{\text{pto}}} \begin{bmatrix} \forall_{\text{out}} \\ I_{\text{out}} \end{bmatrix}, \tag{28}$$

which gives

$$[\mathbf{a}]_{\text{pto}} = \begin{bmatrix} A_{\text{pto}} & B_{\text{pto}} \\ C_{\text{pto}} & D_{\text{pto}} \end{bmatrix} = \begin{bmatrix} \frac{N}{k_\tau} Z_d & k_\tau N + \frac{N}{k_\tau} Z_d Z_w \\ \frac{1}{k_\tau N} & \frac{Z_w}{k_\tau N} \end{bmatrix}. \tag{29}$$

The PTO transmission matrix ($[\mathbf{a}]_{\text{pto}}$) enables direct conversion from electrical to mechanical power variables, and reciprocally, if the mechanical power variables are known, the inverse of (29) allows quick computation of the electrical counterparts. As previously noted, we may readily convert between the impedance and transmission representations for the PTO network via (6).

3.2.3. PTO input and output impedances

As noted in Section 2, a two-port network may be collapsed to a one-port element if one of the ports is terminated with a load and has no independent sources. The "output impedance" of the PTO (Z_{out}) is the impedance as seen by a source connected to the output port of the PTO element (see Figure 5d). As noted, we consider a scenario with no independent sources (i.e., $F_{\text{exc}} = 0$) and express the impedance as the ratio of effort to flow variables at the output port.

$$Z_{\text{out}} = \frac{\forall_{\text{out}}}{I_{\text{in}}}\Big|_{F_{\text{exc}}=0} \tag{30}$$

Recalling (16a), we may rewrite the expression for the first output in (24) as follows.

$$F_{\text{pto}} = Z_{11}v + Z_{12}I_{\text{in}} \tag{31a}$$

$$-v(Z_i + Z_{11}) = Z_{12}I_{\text{in}} \tag{31b}$$

$$\frac{v}{I_{\text{in}}} = -\frac{Z_{12}}{Z_i + Z_{11}} \tag{31c}$$

Similarly, the expression for the second output of (24) may be rearranged as

$$\forall_{\text{out}} = Z_{21}v + Z_{22}I_{\text{in}} \tag{32a}$$

$$\frac{\forall_{\text{out}}}{I_{\text{in}}} = Z_{21}\frac{v}{I_{\text{in}}} + Z_{22}. \tag{32b}$$

Finally, substituting (31c) into (32b) gives an expression for the PTO output port impedance.

$$Z_{\text{out}} = \frac{\forall_{\text{out}}}{I_{\text{in}}}\Big|_{F_{\text{exc}}=0} = Z_{22} - \frac{Z_{12}Z_{21}}{Z_i + Z_{11}} \tag{33}$$

Similarly, the PTO input port's impedance (illustrated in Figure 5e) can be expressed as the ratio of effort (F_{pto}) and flow (v) on the input port. We evaluate this scenario with the input port open and with the output port fully connected such that the load impedance relates the output voltage and current. Substituting (21) into (24) in a manner similar as was done for the output port impedance, we find

$$Z_{\text{in}} = \frac{F_{\text{pto}}}{v} = Z_{11} - \frac{Z_{12}Z_{21}}{Z_\ell + Z_{22}}. \tag{34}$$

As shown in [3], to maximize power transferred to the load, we can apply impedance matching at the input and output ports of the PTO.

$$Z_{\text{in}} = Z_i^* \tag{35a}$$

$$Z_{\text{out}} = Z_\ell^* \tag{35b}$$

From (35), we can explicitly see how different factors of the device design affect impedance matching, which will have a direct effect on power delivered to the load. Utilizing (26), the expressions for Z_{in} and Z_{out} may be expanded, giving us some

insight into the design implications of the bi-conjugate impedance matching condition specified by (35).

$$Z_{\text{out}} = Z_{22} - \frac{Z_{12}Z_{21}}{Z_i + Z_{11}} = Z_w + \frac{k_\tau^2 N^2}{Z_i + Z_d N^2} \qquad (36a)$$

$$Z_{\text{in}} = Z_{11} - \frac{Z_{12}Z_{21}}{Z_\ell + Z_{22}} = Z_d N^2 + \frac{k_\tau^2 N^2}{Z_\ell + Z_w} \qquad (36b)$$

3.2.4. Thévenin equivalent system

Thévenin's theorem [10] states that any linear network may be described by a single source (F_{th}) and impedance (Z_{th}), as shown in Figure 5e. Thévenin equivalent networks for WECs have been considered by a number of authors [11, 3, 12, 13, 14]. Using (16a) and (24), we may write

$$F_{\text{exc}} = Z_i v + Z_{11} v - Z_{12} I_{\text{out}}$$

$$v = \frac{F_{\text{exc}} + Z_{12} I_{\text{out}}}{Z_i + Z_{11}}$$

$$\forall_{\text{out}} = Z_{21}\left(\frac{F_{\text{exc}} + Z_{12} I_{\text{out}}}{Z_i + Z_{11}}\right) - Z_{22} I_{\text{out}}$$

$$= \underbrace{\frac{Z_{21}}{Z_i + Z_{11}} F_{\text{exc}}}_{F_{\text{th}}} + \underbrace{\left(-Z_{22} + \frac{Z_{12}Z_{21}}{Z_i + Z_{11}}\right)}_{-Z_{\text{th}}} I_{\text{out}},$$

which gives

$$Z_{\text{th}} = Z_{22} - \frac{Z_{21}Z_{12}}{Z_i + Z_{11}} \qquad (37a)$$

$$F_{\text{th}} = \frac{Z_{21}}{Z_i + Z_{11}} F_{\text{exc}}. \qquad (37b)$$

Comparing (37a) and (33) along with Figure 5e and our previous discussion about collapsing two-port elements to impedances, it becomes clear that the Thévenin equivalent impedance is equal to the PTO output impedance ($Z_{\text{th}} = Z_{\text{out}}$).

We may consider the well-known impedance matching condition for the Thévenin equivalent system to design an optimal load in order to maximize the power flow from the source to the load.

$$Z_\ell = Z_{\text{th}}^* = Z_{\text{out}}^* \qquad (38)$$

Here, we have restated (35b). Thus, these two modes of representing the system are indeed equivalent and give the same condition for maximum power transfer.

As illustrated in Figure 5, we may represent the WEC system in many different ways (Figure 5a, b, c, and f are all equivalent). These different representations have different utilities. The Thévenin equivalent system in Figure 5f is the most simplified system and gives a clear condition for control design in (38) and a limit for maximum power delivered to the load (see Section 3.2.5). The single two-port representation of the PTO used in Figure 5c provides an additional impedance matching condition in (35), thus more clearly expressing the co-design problem. Figure 5b provides further detail by splitting the PTO into separate drive-train and electric machine two-port elements. While

not explored in this paper, a three-part impedance matching condition could be written for the representation shown in Figure 5b.

3.2.5. Power at the load

Average complex power delivered to the load is defined as

$$\mathcal{S}_\ell = \frac{1}{2} \forall_{\text{out}} I_{\text{out}}^* = \frac{1}{2} Z_\ell I_{\text{out}} I_{\text{out}}^* = \frac{1}{2} Z_\ell |I_{\text{out}}|^2$$
$$= \frac{1}{2} Z_\ell \left| \frac{F_{\text{exc}} Z_{21}}{(Z_\ell + Z_{22})(Z_i + Z_{11}) - Z_{21}Z_{12}} \right|^2 \qquad (39)$$

There are three canonical interpretations of this complex power at the load:

$$\text{Active power: } \mathcal{P}_\ell = \mathfrak{R}\{\mathcal{S}_\ell\} \qquad (40a)$$

$$\text{Reactive power: } Q_\ell = \mathfrak{I}\{\mathcal{S}_\ell\} \qquad (40b)$$

$$\text{Apparent power: } |\mathcal{S}_\ell| \qquad (40c)$$

The active power is power dissipated at the load. Returning to Figure 3, note that we have defined this load as the leads between the motor/generator and the motor controller. Thus, as defined, the active power represents power into the motor controller. Note that there are additional losses and dynamics in the motor controller before power is delivered to the DC bus. However, the motor controller dynamics occur at much higher frequencies than those in the rest of the system. For this reason, we may consider those losses separately and treat the motor controller as a static system (e.g., representing losses in the motor controller as a static function of motor torque and speed).

3.2.6. Performance metrics

A number of performance metrics related to power transfer can now be formulated to inform the design problem. When (35a) is satisfied, maximum power is delivered to the power take-off (the input port of the two-port network) by a wave exerting an excitation force of F_{exc} [8].

$$\mathcal{P}_{\text{in,max}} = \frac{|F_{\text{exc}}|^2}{8\mathfrak{R}\{Z_i\}} \qquad (41)$$

Similarly, when condition (35b) is satisfied, the Thévenin equivalent system gives a clear expression for the maximum power delivered to the load.

$$\mathcal{P}_{\ell,\text{max}} = \frac{|F_{\text{th}}|^2}{8\mathfrak{R}\{Z_{\text{th}}\}} = \left|\frac{Z_{21}}{Z_i + Z_{11}}\right|^2 \frac{|F_{\text{exc}}|^2}{8\mathfrak{R}\{Z_{\text{out}}\}} \qquad (42)$$

In the general case, when (35) is not necessarily satisfied, power delivered to the power take-off ($\mathcal{P}_{\text{in}}$) and power delivered to the load ($\mathcal{P}_\ell$) are as follows.

$$\mathcal{P}_{\text{in}} = \frac{1}{2} v^2 \mathfrak{R}\{Z_{\text{in}}\} \qquad (43a)$$

$$\mathcal{P}_\ell = \frac{1}{2} I_{\text{out}}^2 \mathfrak{R}\{Z_\ell\} \qquad (43b)$$

Using these quantities, we may express three "power gains" (ratios of output power to input power):
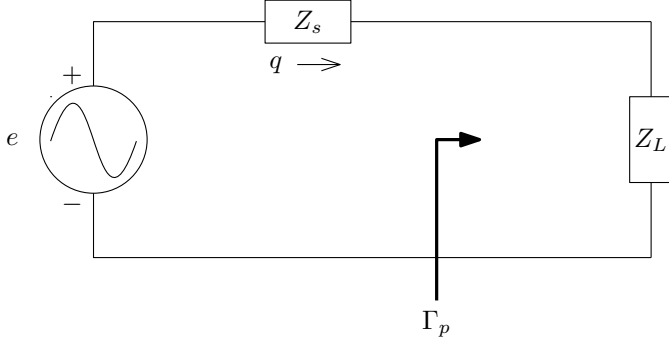
7

Figure 6: Power reflection coefficient (Γ) in a simple system looking from the source impedance (Z_s) towards the load impedance (Z_L).

- Transducer power gain, G_T: the ratio of power delivered to the load to the maximum power available at the source ("wave-to-wire efficiency")

- Available power gain, G_A: the ratio of maximum power delivered to the load to the maximum power available at the source ("ideal wave-to-wire efficiency")

- Operating power gain, G_O: the ratio of power delivered to the load to the power delivered to the power take-off ("PTO efficiency")

$$G_T = \frac{\mathcal{P}_\ell}{\mathcal{P}_{\text{in,max}}} = \frac{4Z_{21}^2 \, \Re\{Z_i\} \, \Re\{Z_\ell\}}{((Z_\ell + Z_{22})(Z_i + Z_{11}) - Z_{12}Z_{21})^2} \tag{44a}$$

$$G_A = \frac{\mathcal{P}_{\ell,\text{max}}}{\mathcal{P}_{\text{in,max}}} = \left(\frac{Z_{21}}{Z_i + Z_{11}}\right)^2 \frac{\Re\{Z_i\}}{\Re\{Z_{\text{out}}\}} \tag{44b}$$

$$G_O = \frac{\mathcal{P}_\ell}{\mathcal{P}_{\text{in}}} = \left(\frac{Z_{21}}{Z_\ell + Z_{22}}\right)^2 \frac{\Re\{Z_\ell\}}{\Re\{Z_{\text{in}}\}} \tag{44c}$$

These power gains are *efficiencies* of the system/subsystems (i.e., they are ratios of power taken at two points in the system). They capture the effect of both *losses* and *reflections*. Power reflection/transmission coefficients consider a single interface and quantify only reflection/transmission at that interface. A typical illustration of a power reflection coefficient (Γ_p) is show in Figure 6, where Γ_p is defined as the ratio of the reflected power to the incident power looking from Z_s towards Z_L [15].

$$\Gamma_p = \left| \frac{Z_L - Z_s^*}{Z_L + Z_s} \right|^2 \tag{45}$$

The fraction of power transmitted (the "power transmission coefficient") is $1 - \Gamma$. We can see from (45) that when the matching condition $Z_L = Z_s^*$ is satisfied, Γ will be zero and all power will be transmitted through the interface in question. Reflection/transmission coefficients may be considered at different points within the system (consider, e.g., Figure 5e, where we may examine power reflection/transmission at the input of the PTO by comparing Z_{in} and Z_i). Note that the power gains and reflection coefficients can also be expressed in terms of the scattering parameters from (7) [6].

$$\Gamma_{p,in} = |S_{11}|^2 \tag{46a}$$

$$\Gamma_{p,out} = |S_{22}|^2 \tag{46b}$$

$$G_T = |S_{21}(Z_s, Z_\ell)|^2 \tag{46c}$$

$$G_A = |S_{21}(Z_s, Z_{\text{out}}^*)|^2 \tag{46d}$$

$$G_O = |S_{21}(Z_{\text{in}}^*, Z_\ell)|^2 \tag{46e}$$

4. Illustrative examples

Many problems in WEC design can be examined through the concepts discussed in Section 3. We will consider a subset of these applications in the subsequent sections.

4.1. Control design

One very relevant and illustrative scenario is that in which the machine design is assumed fixed, and we must maximize performance by setting the load impedance by designing a controller. Many papers in the area of WEC control have focused on this very problem. As discussed in Section 1, the WEC control design problem is often defined to maximize mechanical power ($\mathcal{S}_m$) by satisfying impedance matching at the input of the PTO per (35a).

$$\mathcal{S}_m = \frac{1}{2} F_{\text{pto}} v^* = \frac{1}{2} Z_{\text{in}} v v^* = \frac{1}{2} Z_{\text{in}} |v|^2$$
$$= \frac{1}{2} Z_{\text{in}} \left| \frac{F_{\text{exc}}}{Z_i + Z_{\text{in}}} \right|^2 \tag{47}$$

This disregards the rest of the system and invites possibly deleterious effects, as illustrated in Figure 7, which shows the load impedances and resulting transducer gains for two cases:

- A controller to maximize *mechanical* power: $C|_{Z_{\text{in}}=Z_i^*}$

- A controller to maximize *electrical* power: $C|_{Z_\ell=Z_{\text{out}}^*}$

From Figure 7, we can see that the mechanical power maximizing controller load impedance is notably different from that of the controller that maximizes electrical power. At ~ 0.575 Hz, both controllers have zero phase, but the magnitudes do not match. Away from resonance, the phases of the two controllers differ dramatically. Furthermore, the transducer gain of the two systems are strikingly different, with the gain for the mechanical power maximizing controller *negative* for much of the frequency range – this means the controller designed to *maximize* mechanical power actually *consumes* electrical power.

The results in Figure 7 use theoretical optimal controllers. While higher-order controllers can *approach* a perfect realization of the optimal load impedance per (35b), perfect matching at all frequencies cannot be achieved in practice.[5] However, real

---

[5] Per the Bode-Fano limit, impedance matching can be achieved over only a finite bandwidth – the limit for the matching bandwidth is proportional to the ratio of resistance to reactance in the impedance.
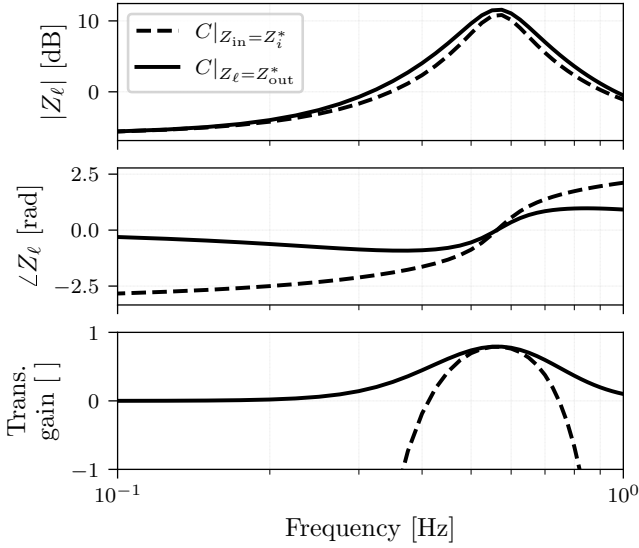
Figure 7: Load impedances (top and middle axes) created by a controller designed to maximize mechanical power ($C|_{Z_{in}=Z_i^*}$, shown with a dashed curve) and a controller designed to maximize electrical power ($C|_{Z_\ell=Z_{out}^*}$, shown with a solid curve) along with the transducer gains (bottom axes) for each controller.
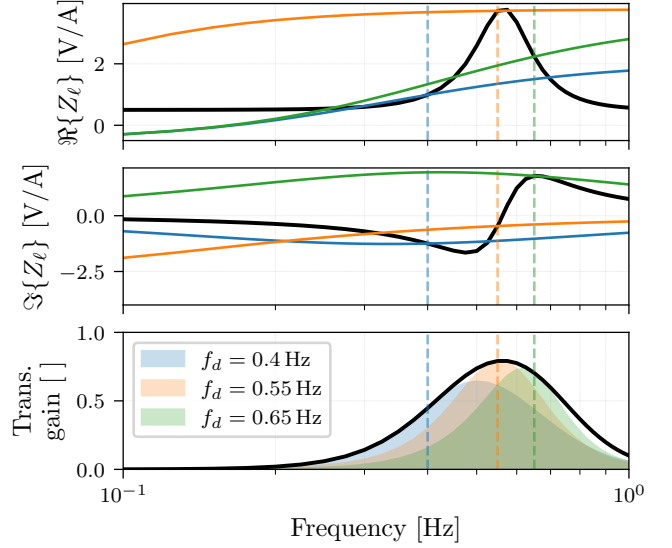

Figure 8: Optimal load impedance (black curve) and load impedances produced by three PI controllers (colored curves) tuned for different design frequencies (dashed vertical lines; $f_d = [0.4, 0.55, 0.65]$ Hz) with corresponding transducer gains.

ocean sea states have relatively narrow bandwidths [9], meaning that a given controller only needs to match the load impedance over a narrow frequency range – the controller may be updated to accommodate changing sea states [16]. These concepts are illustrated in Figure 8, where PI controllers are tuned for waves with frequencies 0.4, 0.55, and 0.65 Hz. While the three controllers each achieve perfect impedance matching at only a single frequency, we can see from the transducer gain that they perform quite well relative to the theoretical optimal over a limited frequency range.

4.2. PTO co-design

From (35), we can see clear guidance for how the machine and controller can be designed to maximize power delivered to the load (i.e., maximize electrical power output). Consider Figure 9, where we separately investigate the effects of adding a negative stiffness element[6] to the drive-train (Figure 9a) and adding inertia to the drive-train (Figure 9b). The left-hand axes in each figure show Z_{in} (colored curves) along with Z_i^* (black dashed curve), which we would like to match by altering the machine design. The right-hand axes in each figure show Z_{out}. In each case, we enforce (35b) such that the theoretical optimal load impedance (Z_ℓ) is used to maximize electrical power.

Both of the considered design alterations (negative stiffness and increased shaft inertia) have the effect of improving impedance matching on the input port at lower frequencies. Recall also that the power transported by an ocean wave is inversely proportional to the wave frequency and that lower frequency

(longer wavelength) waves can grow to larger amplitudes before breaking, meaning that this improved impedance matching at lower frequencies may be particularly advantageous. It should be noted that the range of values for K_d and J_d shown in Figure 9 is somewhat arbitrary and intended only to illustrate trends – one cannot directly compare the effects of doubling the shaft inertia with doubling the negative spring stiffness in terms of an engineering decision. With this in mind, we can see that, for this specific example, adding shaft inertia (Figure 9b) appears to adversely affect the shape of the input impedance (both in terms of the real and imaginary parts) by narrowing the bandwidth over which a good matching with the intrinsic impedance is achieved, whereas adding a negative spring (Figure 9a) appears to have the opposite effect, generally increasing the bandwidth over which good matching with the intrinsic impedance occurs. While we might intuitively expect that changes to K_d and J_d would only affect the imaginary part of the impedances, we can see from Figure 9 and (36) that these terms do indeed affect the real part of the impedances as well.

The resulting performance of these different designs can be characterized using the power reflection coefficient per (45). Figure 10 shows the power reflection coefficient at the input of the PTO. As noted from Figure 9, the negative spring creates a broader impedance matching at the PTO input port, and thus we observe a broader range over which the power reflection at the input of the PTO remains low in the spring designs than in the shaft inertia designs.

Of course, we do not need to apply these design strategies exclusively, and in practice we would consider altering the shaft inertia and negative spring together, along with many other design parameters. Different WEC archetypes will have different design parameters that can be considered through this same lens. For example, the inertia and restoring stiffness of a flap

---

[6]The addition of a negative stiffness element has been applied in WEC design by CorPower in the form of a hydraulic assembly [17] and also by Sandia Labs via a tunable magnetic spring [7].
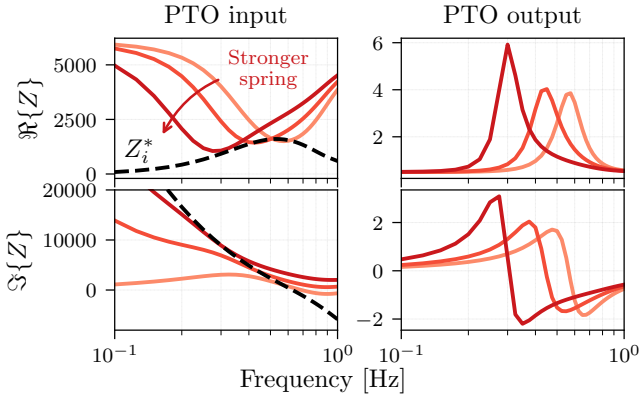
(a) Varying levels of stiffness on shaft ($K_d = [0, -50, -100]$ Nm/rad)
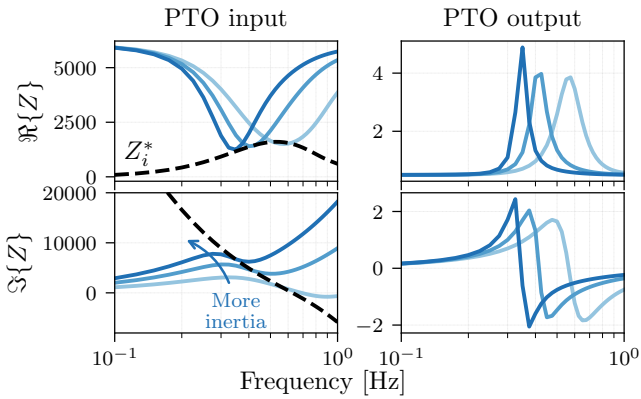
(b) Varying levels of shaft inertia ($I_d = [2, 11, 20]$ kg m^2)

Figure 9: Input port (left) and output port (right) impedances. Upper axes show real part ($\Re\{Z\}$), lower axes show imaginary part ($\Im\{Z\}$). Impedance matching condition on the input port per (35a) illustrated by black dashed curve.

device, along with other properties, will be strongly tied to the height of the flap and its ballasting.

5. Discussion and conclusions

Expanding on [3], this paper casts WEC design as an impedance shaping problem. Sizing/shaping the hull, altering the drive-train, motor/generator selection, control design, and many more factors all have interrelated effects on the impedance matching and therefore on the power delivered to the load. These design considerations can be considered via a wealth of experience and tools developed in other engineering fields for impedance matching problems.

In practice, the bi-conjugate impedance matching requirement expressed by (35) cannot be perfectly satisfied at all frequencies, and the cost of improving the matching condition must be balanced with the resulting benefits. Furthermore, this formulation does not capture constraints (e.g., maximum torque from a generator or maximum travel of a linear piston) and non-linear dynamics, which eventually must be considered. Given these practical considerations, numerical optimization becomes
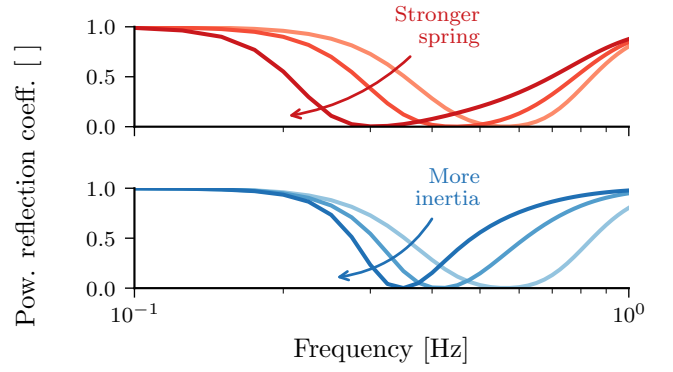

Figure 10: Power take-off input power reflection coefficients for different levels of spring stiffness (top axes with red curves; $K_d = [0, -50, -100]$ Nm/rad) and shaft inertia (bottom axes with blue curves; $I_d = [2, 11, 20]$ kg m^2).

a useful tool. Nonetheless, the linear modeling approach presented here provides a critical starting point and foundation to build from.

6. Acknowledgements

Appendix A. Multi-port network impedance matching conventions

Multi-port networks are applied across a wide variety of fields, in which a number of conventions and underlying assumptions are utilized. Two important conventions warrant discussion here:

- **Sign conventions:** Throughout literature, there are many different sign conventions utilized for multi-port systems. In Figure 5a, we define v_s and I_{out} as vectors leaving the two-port elements. This convention is beneficial in two ways:

    - To ensure consistency when cascading two-ports, e.g., when using the *ABCD* formulation.

    - This is the power industry's preferred convention, often referred to as the "passive sign convention" [5]: flow entering through the positive polarity of an element implies that the element is absorbing power.

Yet, to follow the convention for standard two-port networks, we define the flow variables q as vectors entering both sides of the two-port, as shown in Figure 2 and (2). As a result, the impedance matrix and the transmission matrix follow the formulas found in most textbooks.

- **Complex source impedance:** It is common in many fields to assume a real source impedance (typically $50\,\Omega$) [15], however the "source impedance" for a WEC in the formulation presented here is the intrinsic impedance, which is complex. We have therefore presented expressions that do not assume a real source impedance.

- **Scattering parameters:** There are at least three commonly used definitions for scattering parameters [15, 6]. The "Kurokawa power wave scattering parameters" consider power and reference arbitrary complex source/load impedances, this formulation is used in this paper accordingly.

References

[1] J. Falnes, Radiation impedance matrix and optimum power absorption for interacting oscillators in surface waves, Applied Ocean Research 2 (2) (1980) 75–80. doi:10.1016/0141-1187(80)90032-2.
URL https://www.sciencedirect.com/science/article/pii/0141118780900322

[2] D. V. Evans, A theory for wave-power absorption by oscillating bodies, Journal of Fluid Mechanics 77 (1) (1976) 1–25. doi:10.1017/S0022112076001109.
URL https://doi.org/10.1017/S0022112076001109

[3] G. Bacelli, R. G. Coe, Comments on control of wave energy converters, IEEE Transactions on Control Systems Technology 29 (1) (2021) 478–481. doi:10.1109/TCST.2020.2965916.
URL https://ieeexplore.ieee.org/document/9005201

[4] G. Marrocco, The art of UHF RFID antenna design: impedance-matching and size-reduction techniques, IEEE Antennas and Propagation Magazine 50 (1) (2008) 66–79. doi:10.1109/MAP.2008.4494504.
URL https://ieeexplore.ieee.org/abstract/document/4494504

[5] C. K. Alexander, M. N. Sadiku, M. Sadiku, Fundamentals of electric circuits, McGraw-Hill Higher Education Boston, MA, USA, 2007.

[6] S. Amakawa, Scattered reflections on scattering parameters – demystifying complex-referenced s parameters–, IEICE Transactions on Electronics 99 (10) (2016) 1100–1112. doi:10.1587/transele.E99.C.1100.

[7] D. D. Forbush, R. G. Coe, T. Donnelly, R. G. Coe, D. Gallegos-Patterson, S. J. Spencer, J. Spinneken, J. Lee, R. Crandell, K. Dullea, MASK4 test report, Tech. Rep. SAND-2024-00121, Sandia National Laboratories, Albuquerque, NM (January 2024). doi:10.2172/2280836.
URL https://www.osti.gov/biblio/2280836

[8] J. Falnes, Ocean Waves and Oscillating Systems, Cambridge University Press, Cambridge; New York, 2002.

[9] R. G. Coe, G. Bacelli, D. Forbush, A practical approach to wave energy modeling and control, Renewable and Sustainable Energy Reviews 142 (2021) 110791. doi:10.1016/j.rser.2021.110791.
URL https://www.sciencedirect.com/science/article/pii/S1364032121000861

[10] L. Thévenin, Sur un nouveau théoreme d'électricité dynamique [on a new theorem of dynamic electricity], CR des Séances de l'Académie des Sciences 97 (159-161) (1883) 250.

[11] R. McCabe, M. N. Haji, Force-limited control of wave energy converters using a describing function linearization, in: 15th IFAC Conference on Control Applications in Marine Systems, Robotics and Vehicles (IFAC-CAMS), Blacksburg, VA, 2024.

[12] M. Blanco, M. Lafoz, D. Ramirez, G. Navarro, J. Torres, L. García-Tabares, Dimensioning of point absorbers for wave energy conversion by means of differential evolutionary algorithms, IEEE Transactions on Sustainable Energy 10 (3) (2019) 1076–1085. doi:10.1109/TSTE.2018.2860462.
URL https://ieeexplore.ieee.org/document/8421039

[13] K. Bubbar, B. Buckham, P. Wild, A method for comparing wave energy converter conceptual designs based on potential power capture, Renewable Energy 115 (2018) 797–807. doi:10.1016/j.renene.2017.09.005.
URL https://www.sciencedirect.com/science/article/pii/S096014811

[14] T. M. Lewis, B. Bosma, A. von Jouanne, T. K. A. Brekken, Modeling of a two-body wave energy converter driven by spectral JONSWAP waves, in: 2013 IEEE Energy Conversion Congress and Exposition, 2013, pp. 329–336. doi:10.1109/ECCE.2013.6646719.
URL https://ieeexplore.ieee.org/document/6646719

[15] K. Kurokawa, Power waves and the scattering matrix, IEEE Transactions on Microwave Theory and Techniques 13 (2) (1965) 194–202. doi:10.1109/TMTT.1965.1125964.

[16] D. D. Forbush, G. Bacelli, S. J. Spencer, R. G. Coe, D. G. Wilson, B. Robertson, A self-tuning WEC controller for changing sea states, International Marine Energy Journal 5 (3) (2022) 327–338. doi:10.36688/imej.5.327-338.
URL https://marineenergyjournal.org/imej/article/view/70

[17] J. H. Todalshaug, G. S. Ásgeirsson, E. Hjálmarsson, J. Maillet, P. Möller, P. Pires, M. Guérinel, M. Lopes, Tank testing of an inherently phase-controlled wave energy converter, International Journal of Marine Energy 15 (2016) 68–84, selected Papers from the European Wave and Tidal Energy Conference 2015, Nante, France. doi:10.1016/j.ijome.2016.04.007.
URL https://www.sciencedirect.com/science/article/pii/S221416691